Supplementary Information

High-entropy LDH coupled with Ru nanoclusters for efficient overall seawater split-ting

Xiaolin Li [a, #], Ruixing Tang [a, #], Jnxuan Liu[a], Ying Li [a], Limin Liang [a], Wenjie Huang [b,*], Qiuyan Hao [a], Hui Liu [a,*]

a. Key Laboratory of Special Functional Materials for Ecological Environment and Information (Ministry of Education), School of Material Science and Engineering, Hebei University of Technology, Tianjin 300130, P. R. China;

b. School of Materials Science and Engineering, State Key Laboratory of Tropic Ocean Engineering Materials and Materials Evaluation, Key Laboratory of Pico ElectronMi-croscopy of Hainan Province, Hainan University, Haikou 570228, P. R. China.

* Corresponding author.

Hui Liu: liuhuihebut@163.com (e-mail)

Experimental Section

1. Chemicals and materials

The chemical reagents including $Ni(NO_3)_2 \cdot 6H_2O$, $Fe(NO_3)_2 \cdot 9H_2O$, $Co(NO_3)_2 \cdot 6H_2O$, $Mn(NO_3)_2 \cdot 4H_2O$, $Cu(NO_3)_2 \cdot 3H_2O$, and $RuCl_3$ (Ru content 45–55%) were obtained from Aladdin. NH_4F and urea were purchased from Macklin. NaBH4 and $C_6H_5Na_3O_7 \cdot 2H_2O$ were sourced from Innochem.

2. Preparation process of catalyst

Preparation of MnFeCoNiCu LDH

MnFeCoNiCu LDH was synthesized via a hydrothermal method. First, $Ni(NO_3)_2 \cdot 6H_2O$ (0.45 mmol), $Fe(NO_3)_2 \cdot 9H_2O$ (0.45 mmol), $Co(NO_3)_2 \cdot 6H_2O$ (0.45 mmol), $Mn(NO_3)_2 \cdot 4H_2O$ (0.45 mmol), $Cu(NO_3)_2 \cdot 3H_2O$ (0.45 mmol), NH_4F (4 mmol), and urea (10 mmol) were dissolved in 35 mL of deionized water. The mixture was stirred for 30 minutes until complete dissolution. The resulting solution was then transferred into a Teflon-lined autoclave, into which two pieces of pretreated carbon cloth (CC) were placed. The autoclave was sealed and heated at 120 °C for 6 hours.

Preparation of Ru NCs/MnFeCoNiCu LDH

$C_6H_5Na_3O_7 \cdot 2H_2O$ (0.117 g) and $RuCl_3$ (6 mg) were dissolved in 40 mL of deionized water and stirred until completely dissolved. Then, the carbon cloth loaded with MnFeCoNiCu LDH was immersed in the solution and stirred for 5 minutes. Subsequently, the reducing agent $NaBH_4$ (0.01 g) was added into the stirred solution. Finally, the mixture was stirred at room temperature for 30 minutes to allow the deposition of Ru onto the MnFeCoNiCu LDH, successfully obtaining Ru NCs/MnFeCoNiCu LDH.

3. Material characterization

X-ray diffraction (XRD) data were collected using an X-ray diffractometer (Rigaku SmartLab) with Cu Kα radiation (λ = 1.5418 Å). Laser Raman spectroscopy was performed on a HORIBA LabRAM HR Evolution spectrometer using a 532 nm laser to obtain information about the material. Scanning electron microscopy (SEM) images were acquired on an S-4800 field-emission scanning electron microscope operated at an accelerating voltage of 5 kV. Transmission electron microscopy (TEM) data were obtained using a JEM-2100F (JEOL) transmission electron microscope. High-resolution information and X-ray photoelectron spectroscopy (XPS) spectra were measured on a Thermo Scientific K-Alpha X-ray photoelectron spectrometer.

4. Electrochemical test characterization

Electrochemical measurements were conducted at 298 K using a CHI660E electrochemical workstation with a standard three-electrode system. A Hg/HgO electrode was used as the reference electrode, a platinum plate as the counter electrode, and a 1×1 cm^{-2} carbon cloth loaded with the catalyst as the working electrode. The reversible hydrogen electrode (RHE) potential was calculated using the following equation: E(RHE) = E(SHE) + 0.098 + 0.059 × pH. A 1 M KOH + 0.5 M NaCl solution was employed as the electrolyte for seawater testing. Prior to electrochemical performance tests, cyclic voltammetry (CV) was performed at scan rates of 100 mV s^{-1} and 20 mV s^{-1}. Linear sweep voltammetry (LSV) was measured at a scan rate of 2 mV s^{-1} with 95% iR compensation. The solution resistance was measured to be 2.0 Ω.

The double-layer capacitance (C_{dl}) was obtained from CV curves at various scan

rates. The electrochemical surface area (ECSA) of the sample was derived from C_{dl} according to the following equation: ECSA = C_{dl} / C_s, where C_s is taken as 40 μF cm^{-2}. Electrochemical impedance spectroscopy (EIS) spectra were recorded at 1.48 V (vs. RHE) and -0.16 V (vs. RHE) over a frequency range of 10^6 to 10^{-1} Hz.

The stability of the material was evaluated by chronopotentiometry at a current density of 300 mA cm^{-2}. Stability tests for the oxygen evolution reaction (OER) and hydrogen evolution reaction (HER) were carried out in a three-electrode system, while overall water splitting stability tests were performed in a two-electrode system. The Faradaic efficiency of the material was measured using the water displacement gas collection method under multiple current steps.

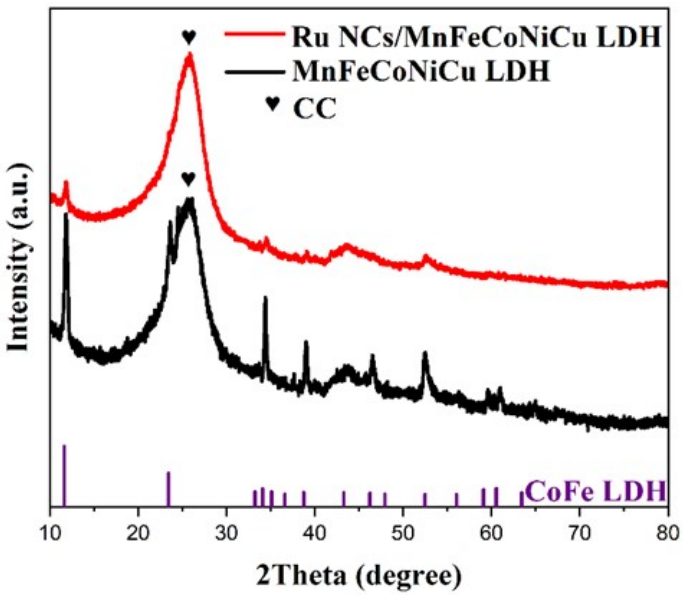

Figure S1. XRD patterns of Ru NCs/MnFeCoNiCu LDH and MnFeCoNiCu LDH.

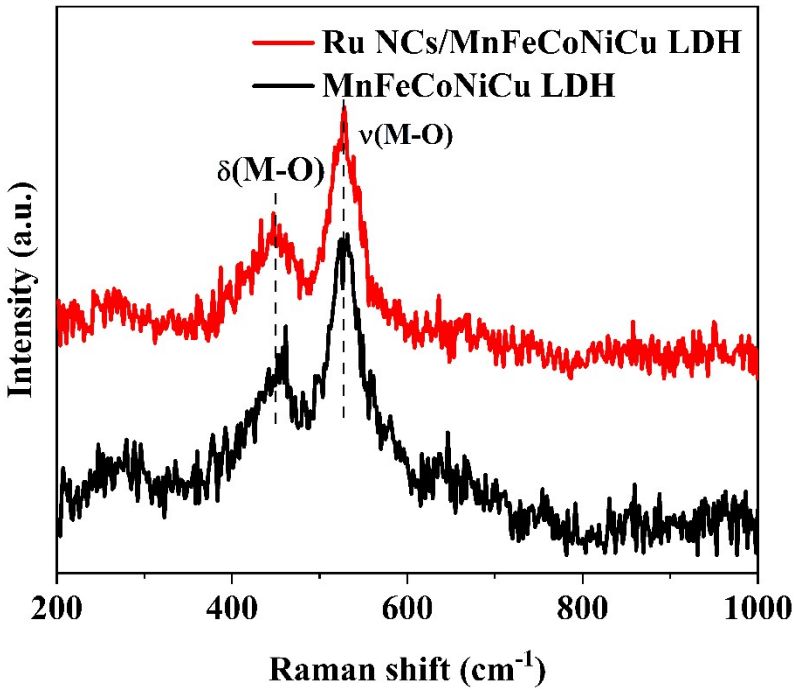

Figure S2. Raman spectra of Ru NCs/MnFeCoNiCu LDH and MnFeCoNiCu LDH.

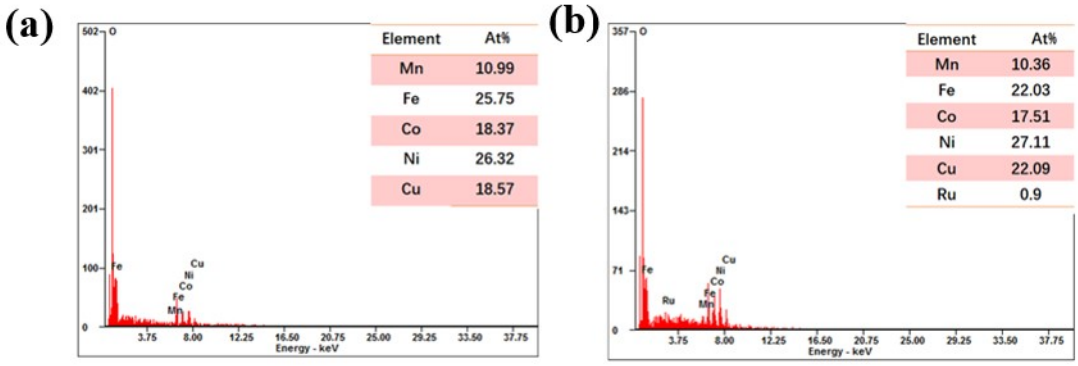

Figure S3. EDS mapping of (a) MnFeCoNiCu LDH and (b) Ru NCs/MnFeCoNiCu LDH.

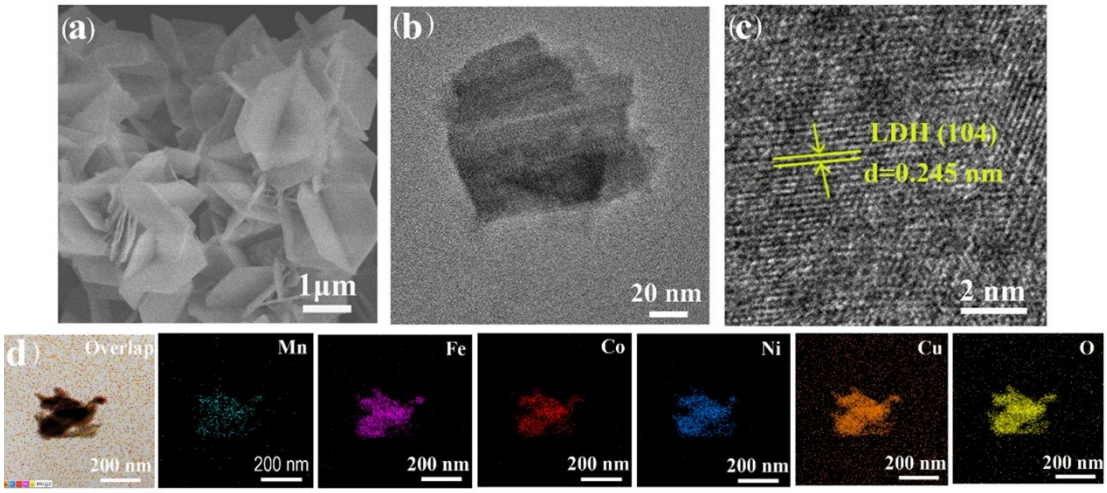

Figure S4. MnFeCoNiCu LDH: (a) SEM image, (b) TEM image, (c) HRTEM image, and (d) Elemental mapping.

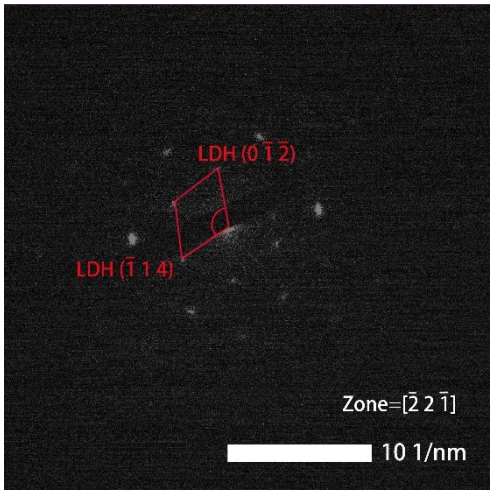

Figure S5. SAED pattern of Ru NCs/MnFeCoNiCu.

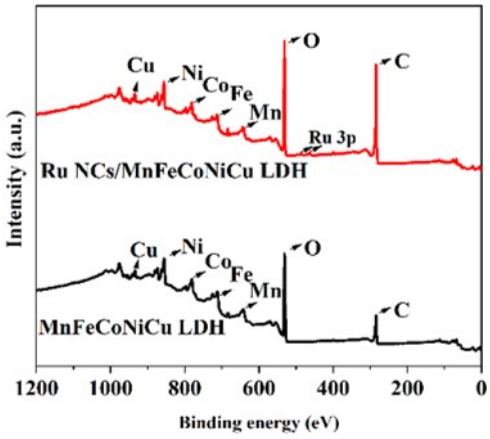

Figure S6. XPS survey spectra of Ru NCs/MnFeCoNiCu LDH and MnFeCoNiCu LDH.

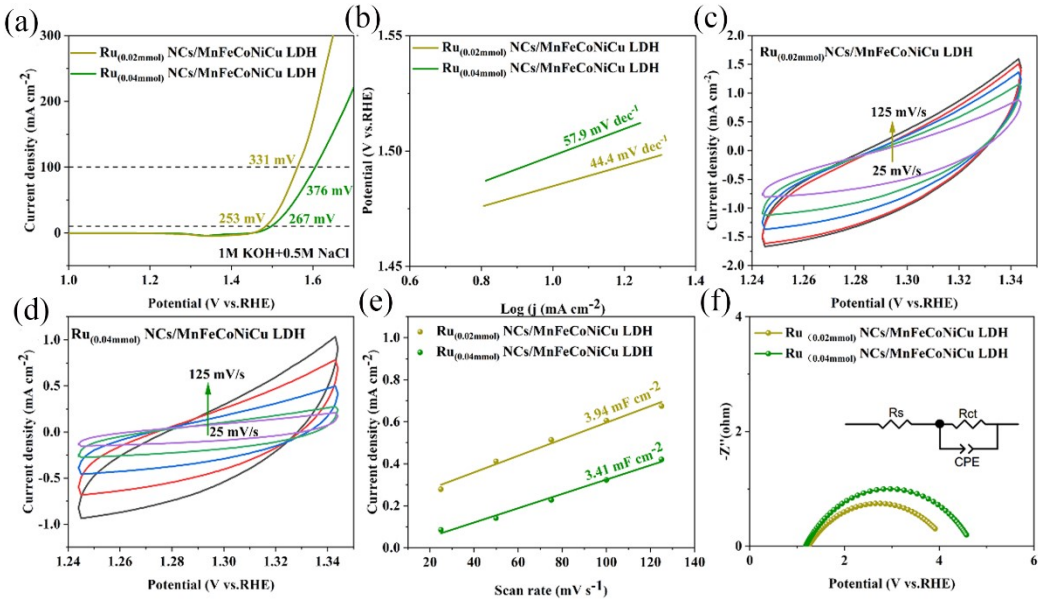

Figure S7.OER performance of Ru NCs/MnFeCoNiCu LDH with Ru loadings of 0.02 mmol and 0.04 mmol. (a) LSV curves, (b) Tafel plots, (c) CV curves of Ru(0.02 mmol) NCs/MnFeCoNiCu LDH at scan rates ranging from 25 to 125 mV s^{-1}, (d) CV curves of Ru(0.04 mmol) NCs/MnFeCoNiCu LDH at scan rates ranging from 25 to 125 mV s^{-1}, (e) Cdl, and (f) EIS.

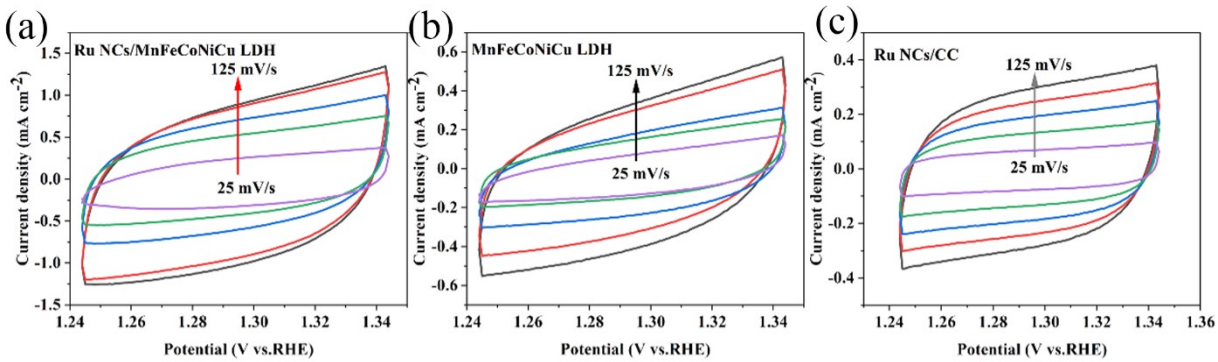

Figure S8. CV curves (OER) for (a) Ru NCs/MnFeCoNiCu LDH, (b) MnFeCoNiCu LDH, and (c) Ru NCs/CC at scan rates ranging from 25 to 125 mV s^{-1}.

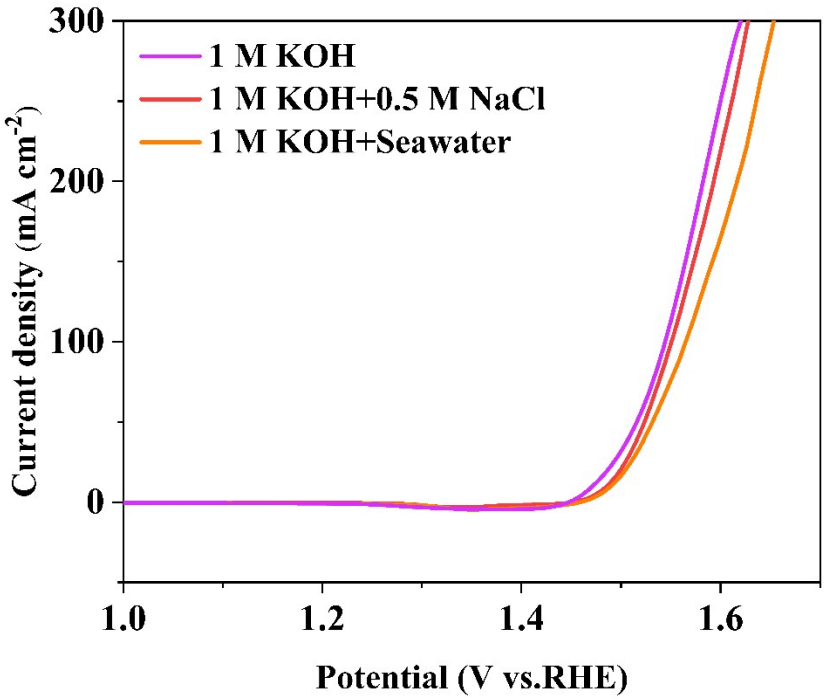

Figure S9. OER activity of Ru NCs/MnFeCoNiCu LDH in pure water, simulated seawater, and real seawater.

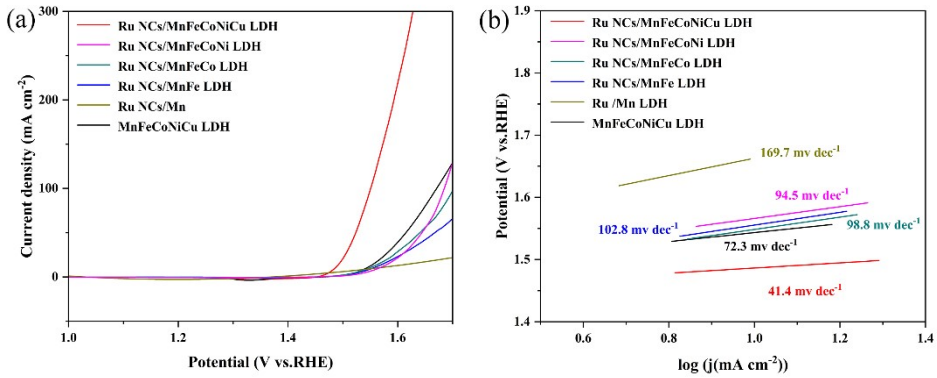

Figure S10. Electrocatalytic performance of Ru NCs/MnFeCoNiCu LDH、Ru NCs/MnFeCoNi LDH、Ru NCs/MnFeCo LDH、Ru NCs/MnFe LDH、Ru NCs/Mn and MnFeCoNiCu LDH (a) LSV in 1 M KOH, (b) Tafel plots

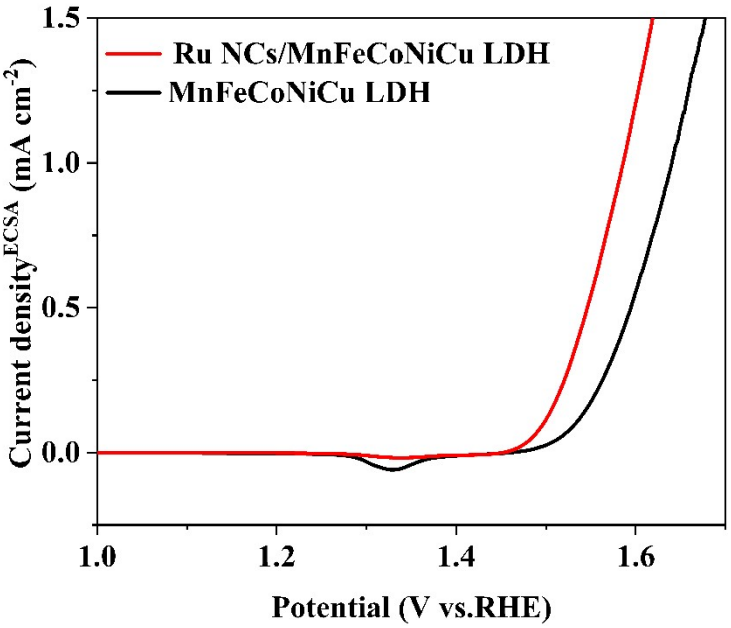

Figure S11. ECSA-normalized intrinsic OER activity of Ru NCs/MnFeCoNiCu LDH.

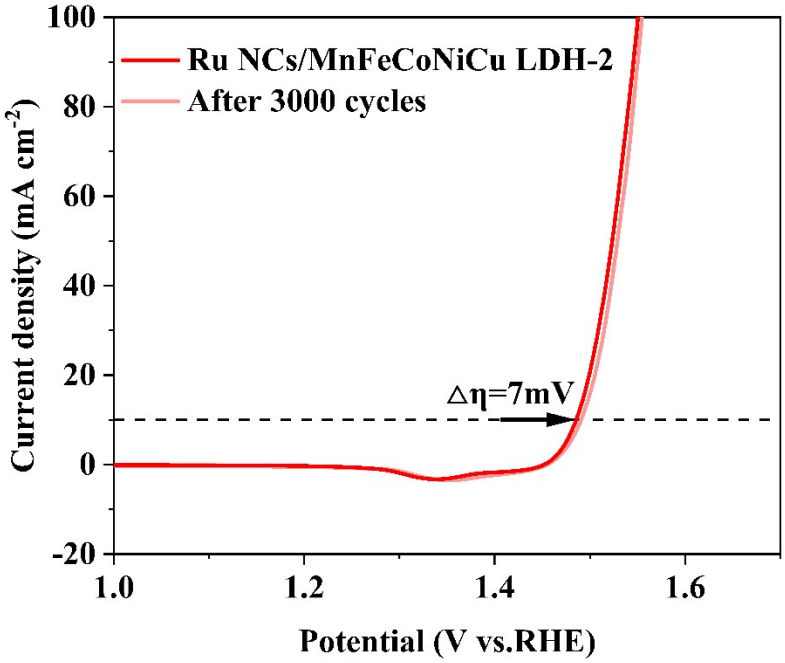

Figure S12. LSV curves of Ru NCs/MnFeCoNiCu LDH for OER before and after 3000 CV cycles.

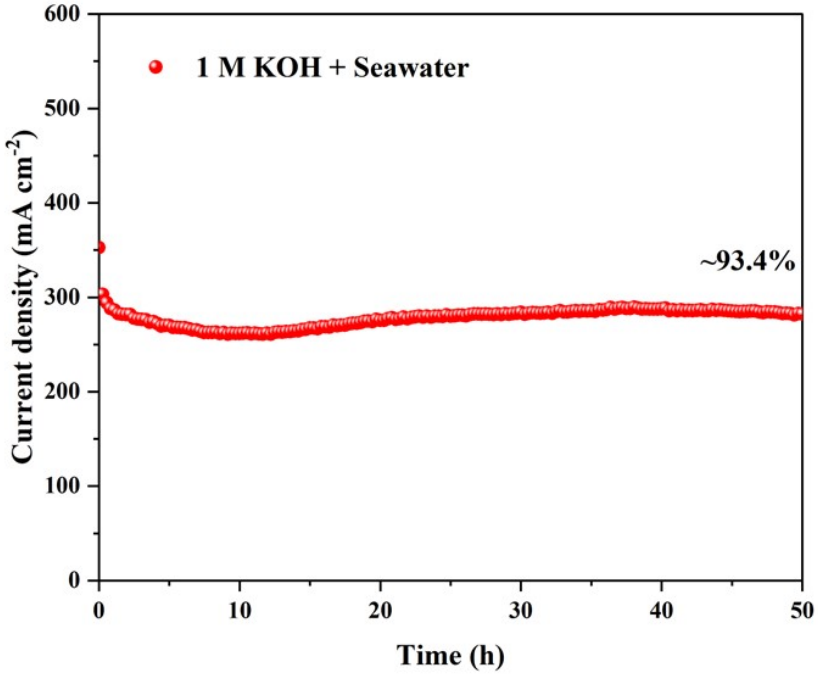

Figure S13. OER stability of Ru NCs/MnFeCoNiCu LDH in real seawater.

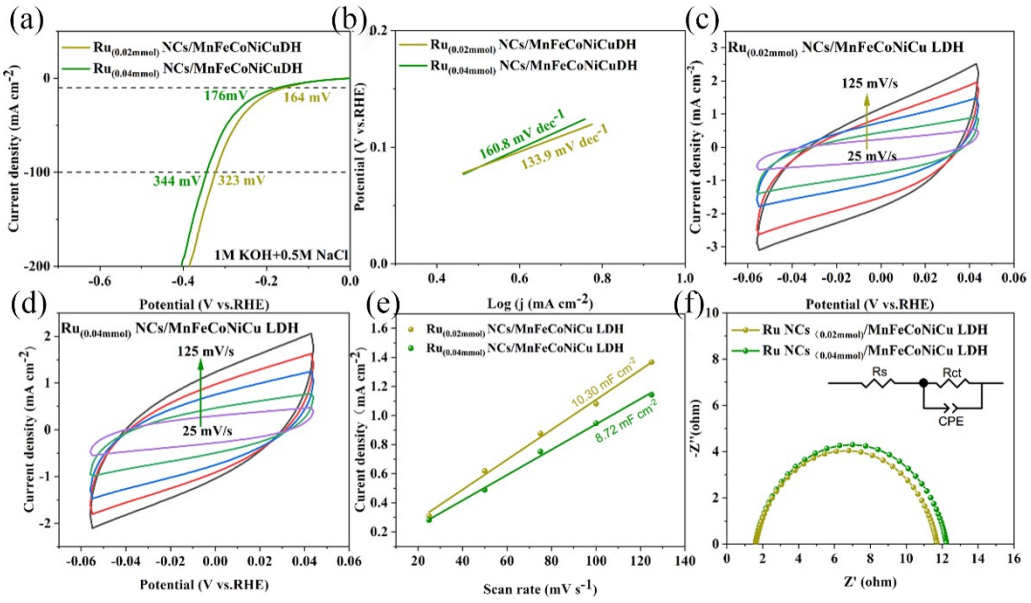

Figure S14. HER performance of Ru NCs/MnFeCoNiCu LDH with Ru loadings of 0.02 mmol and 0.04 mmol. (a) LSV curves, (b) Tafel plots, (c) CV curves of Ru(0.02 mmol) NCs/MnFeCoNiCu LDH at scan rates ranging from 25 to 125 mV s^{-1}, (d) CV curves of Ru(0.04 mmol) NCs/MnFeCoNiCu LDH at scan rates ranging from 25 to 125 mV s^{-1}, (e) Cdl, and (f) EIS.

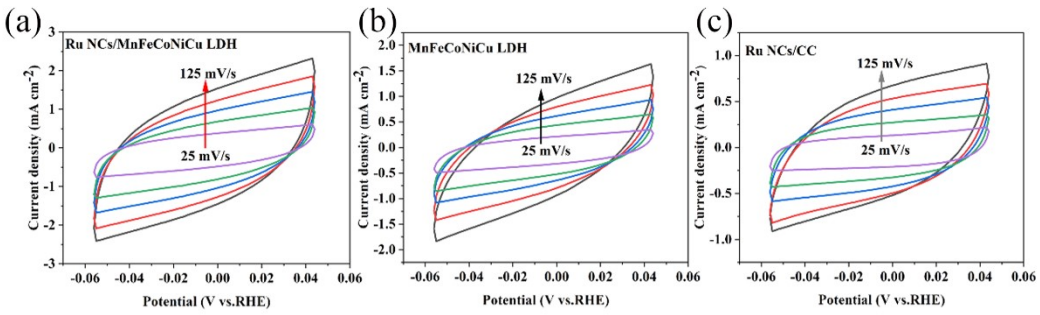

Figure S15. CV curves (HER) for (a) Ru NCs/MnFeCoNiCu LDH, (b) MnFeCoNiCu LDH, and (c) Ru NCs/CC at scan rates ranging from 25 to 125 mV s^{-1}.

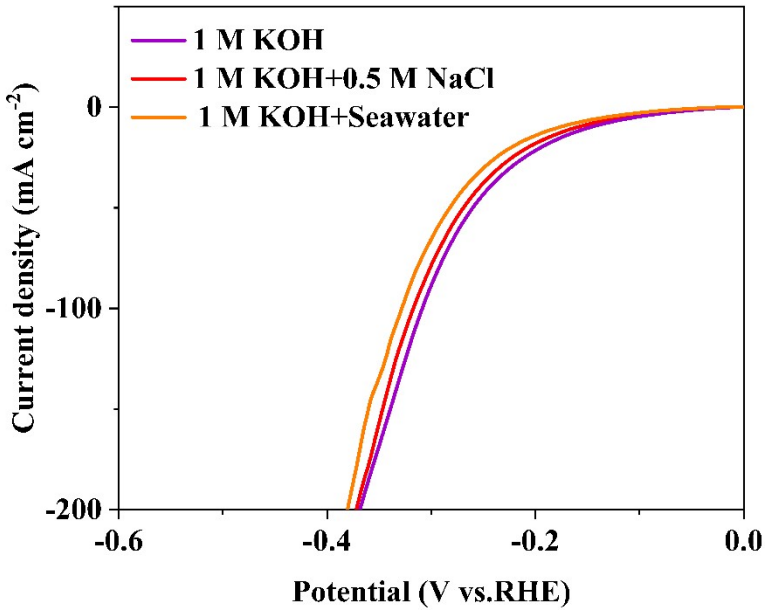

Figure S16. HER activity of Ru NCs/MnFeCoNiCu LDH in pure water and seawater.

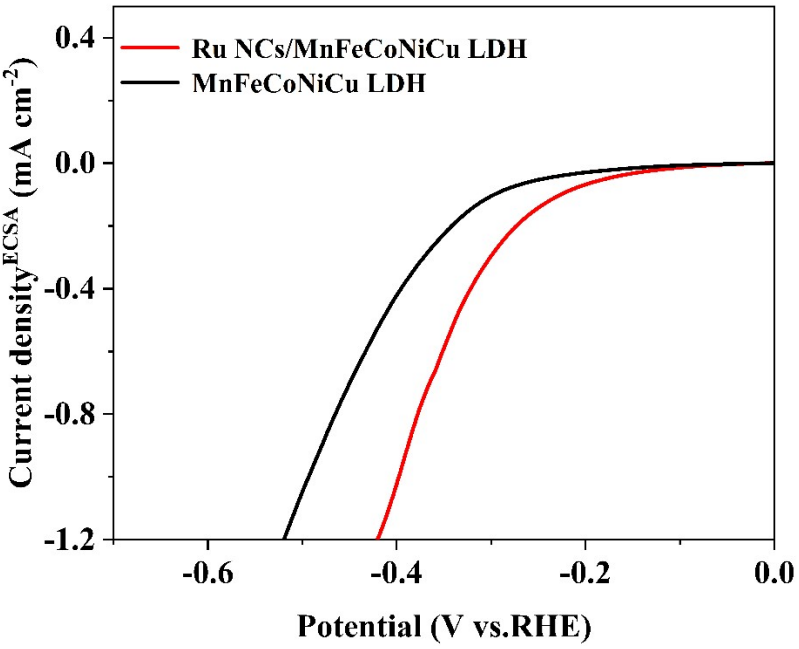

Figure S17. ECSA-normalized intrinsic HER activity of Ru NCs/MnFeCoNiCu LDH.

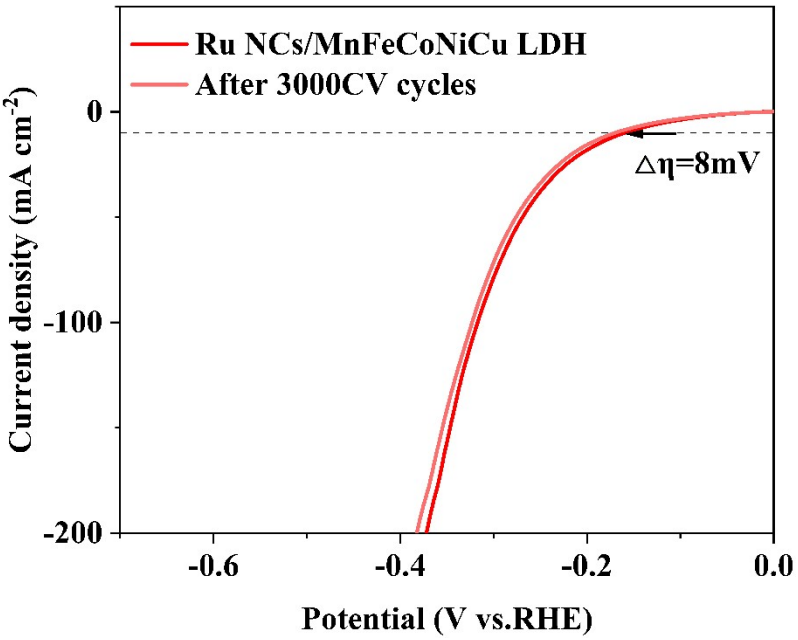

Figure S18. LSV curves of Ru NCs/MnFeCoNiCu LDH for HER before and after 3000 CV cycles.

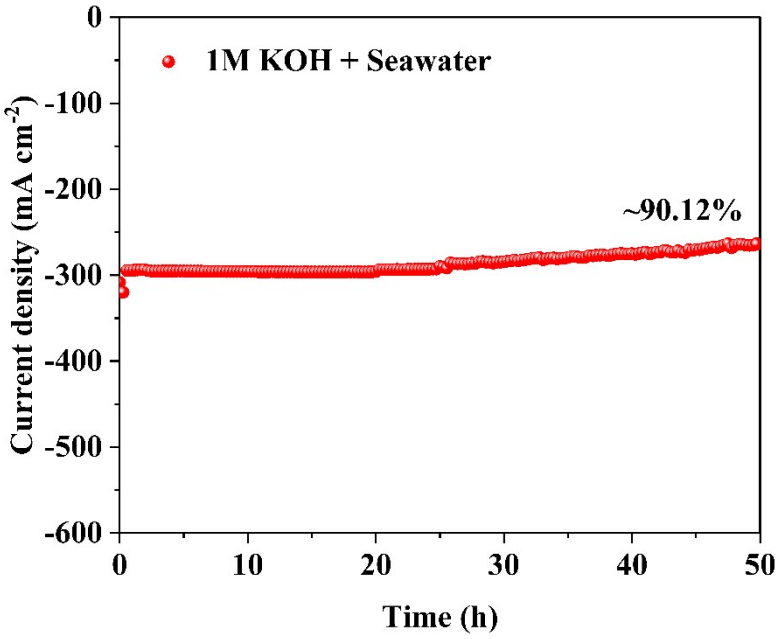

Figure S19. HER stability of Ru NCs/MnFeCoNiCu LDH in real seawater.

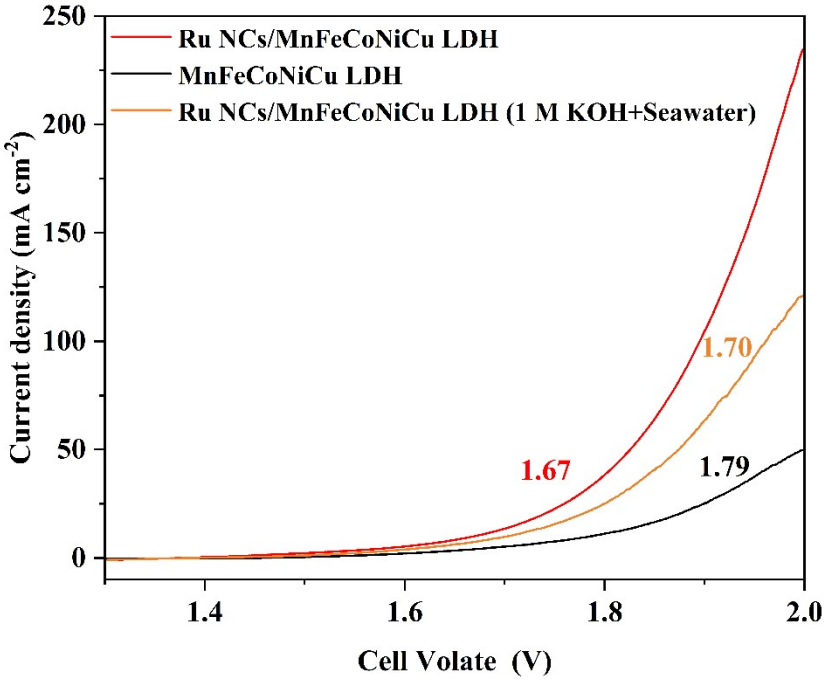

Figure S20. LSV curves for overall water splitting of Ru NCs/MnFeCoNiCu LDH.

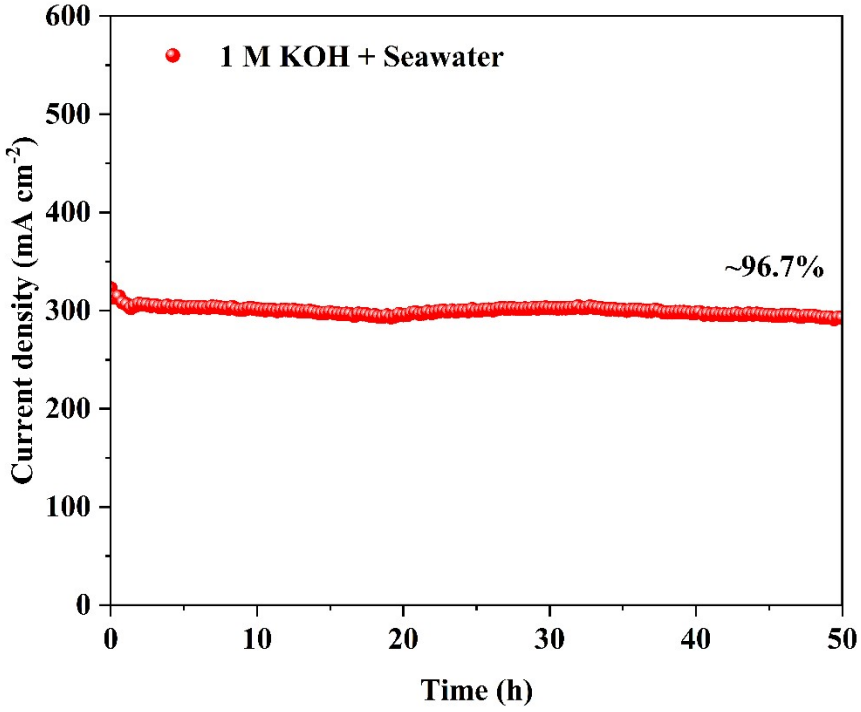

Figure S21. Overall water splitting stability of Ru NCs/MnFeCoNiCu LDH.

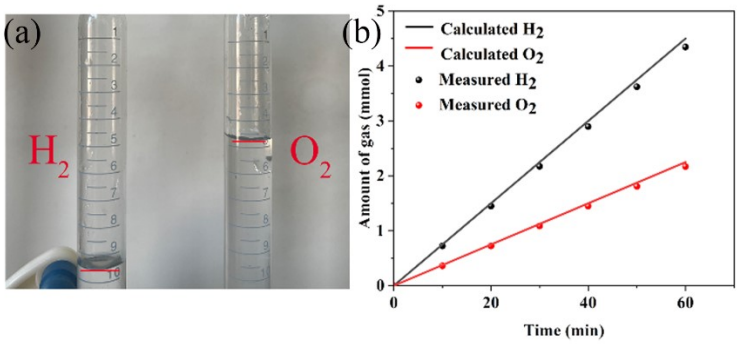

Figure S22. (a) Schematic of the Faraday device (left for hydrogen generation, right for oxygen generation), and (b) Faradaic efficiency.

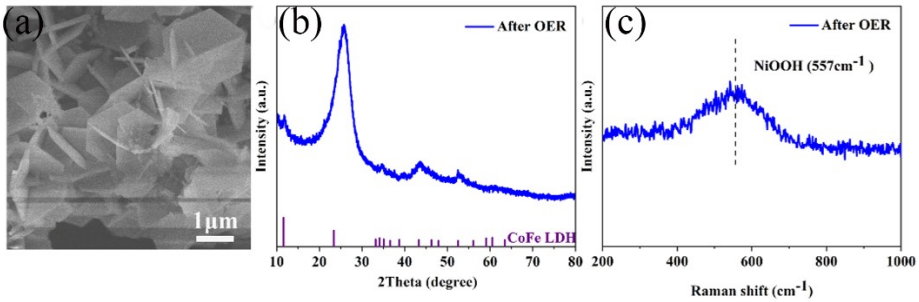

Figure S23. (a) SEM image, (b) XRD pattern, and (c) Raman spectrum of Ru NCs/MnFeCoNiCu LDH after OER.

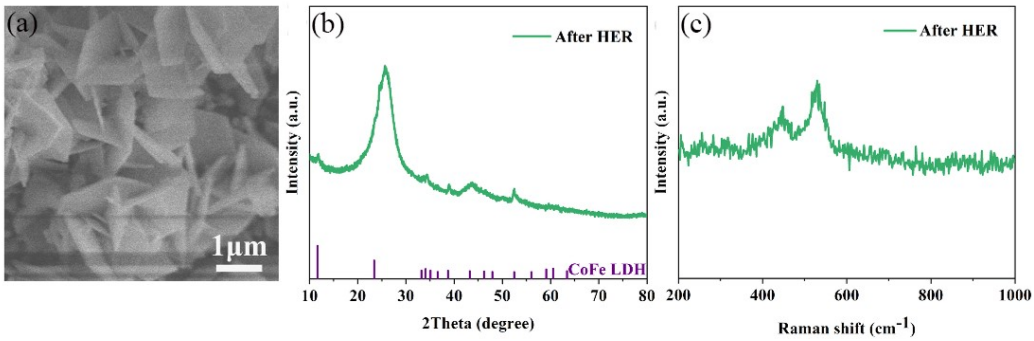

Figure S24. (a) SEM image, (b) XRD pattern, and (c) Raman spectrum of Ru NCs/MnFeCoNiCu LDH after HER.

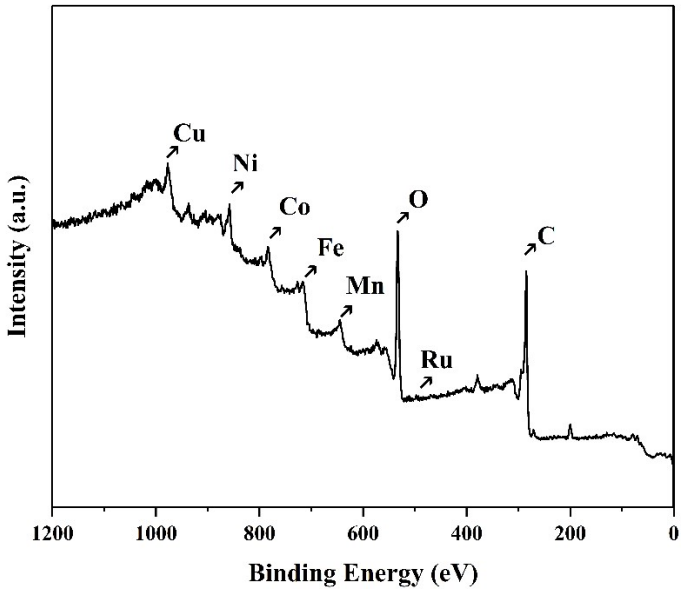

Figure S25. XPS survey spectrum of Ru NCs/MnFeCoNiCu LDH after stability testing

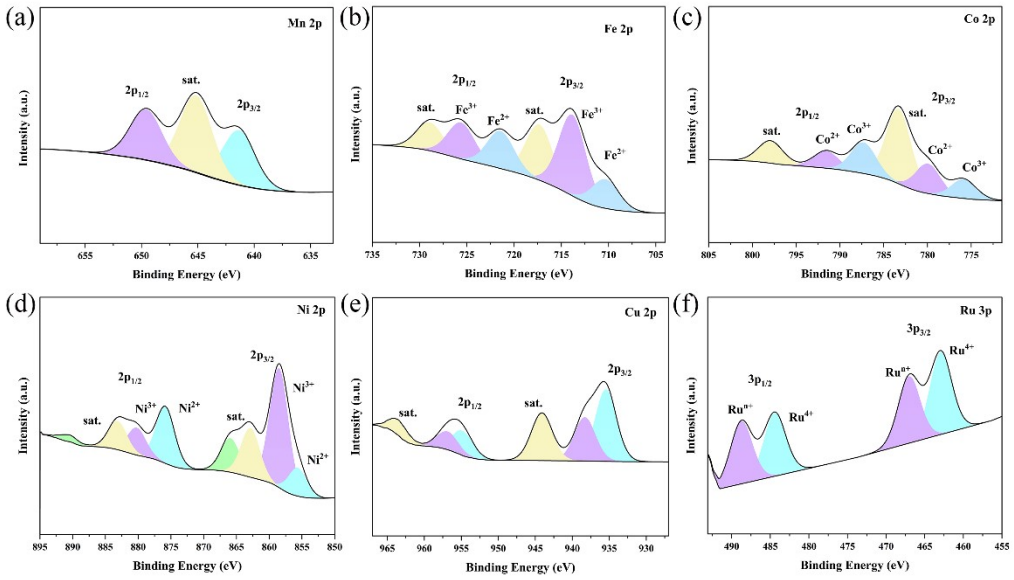

Figure S26. XPS spectra of Ru NCs/MnFeCoNiCu LDH after stability testing: (a) Mn 2p, (b) Fe 2p, (c) Co 2p, (d) Ni 2p, (e) Cu 2p, (f) Ru 3p.

Electrocatalysts	Electrolyte	Overpotentials (mV)	Reference
Ru NCs/MnFeCoNiCu LDH	1.0 M KOH in seawater	170 (10 mA cm^{-2})	This work
Ru/CoMoOx@CC	1.0 M KOH in seawater	78 (10 mA cm^{-2})	S1
Cu@1T-N-W NS	1.0 M KOH in seawater	158 (10 mA cm^{-2})	S2
$NiSe_2$	1.0 M KOH in seawater	149 (10 mA cm^{-2})	S3
CuCoCrRuMo HEA	1.0 M KOH in seawater	402 (1000 mA cm^{-2})	S4
FeCoS/Ni/BDD	1 M KOH in seawater	360 (10 mA cm^{-2})	S5
NiCo-ZIF8-P950	1.0 M KOH in seawater	130 (20 mA cm^{-2})	S6
NiSe@$CoSe_2$	1 M KOH in seawater	170 (10 mA cm^{-2})	S7
Fe（10）-VS_2	1 M KOH in seawater	256 (20 mA cm^{-2})	S8
MnO2/MoS2	1.0 M KOH in seawater	131 (10 mA cm^{-2})	S9
CoMoO4@MoP-CoP/NF	1.0 M KOH in seawater	196 (100 mA cm^{-2})	S10
NiFe-LDH-4	1 M KOH in seawater	235 (50 mA cm^{-2})	S11

Table S1. HER activities of various reported catalysts in alkaline simulated

S1 H. Eom, S.-I. Kim, N. Jeong, K. S. Hwang, E.-J. Jwa, Y.-C. Jeung, Y. S. Mok and J.-H. Han, Applied Surface Science, 2025, 707, 163534.

S2 M. Prasanna, H. B. Kwak, M. J. Oh and D. J. Yoo, Inorg. Chem. Front., 2024, 11, 5612–5623.

S3 S. Zhang, R.-Y. Li, X. Li, Y. Tian, R. Zhao, J. Xiang, F. Wu and D. Zhao, Materials Research Bulletin, 2025, 189, 113463.

S4 H. He, Z. Chen, W. Ma, Q. Chen, Q. Li, X. Lv and J. Dang, Acta Materialia, 2026, 307, 121971.

S5 M. Li, G. Chu, J. Gao, X. Ye, M. Hou, S. Guo, Y. Li, Z. Zhou, L. Yang and P. Briois, Sci Rep, 2025, 15, 2862.

S6 F. Zulfiqar, I. Ullah, A. Zahid, M. A. Rafiq and F. Sher, ACS Appl. Energy Mater., 2026, 9, 3443–3454.

S7 Y. Cheng, L. Sui, X. Guo, D. Yang, S. Du and L. Miao, Energy Fuels, 2026, 40, 721–729.

S8 R. R. Arunya, N. N. Abu, J. Valiyaveetil and A. Ganesan, ACS Appl. Nano Mater., 2026, 9, 1113–1128.
S9 R. Shilpa, A. C. Anand, K. S. Sibi, S. R. S. Kumar and R. B. Rakhi, International Journal of Hydrogen Energy, 2025, 117, 73–85.
S10 S. Qiao, C. Rao, H. Chen, M. Xiong, W. Han, Q. Xu, S. Ci and Z. Wen, International Journal of Hydrogen Energy, 2025, 145, 842–850.
S11 X. Li, S. Xu, J. Li, S. Zhang, B. Zhang, R. Zhao, D. Zhao and F. Wu, Nanoscale Adv., 2025, 7, 5546–5560.